Model studies of nonadiabatic dynamics

Daniela Kohen[a)]
Lucent Technologies, Bell Laboratories, Murray Hill, New Jersey 07974

Frank H. Stillinger
Lucent Technologies, Bell Laboratories, Murray Hill, New Jersey 07974 and Princeton Materials Institute, Princeton University, Princeton, New Jersey 08544

John C. Tully
Chemistry Department, Yale University, New Haven, Connecticut 06511

(Received 23 January 1998; accepted 19 June 1998)

Mixed quantum-classical methods are applied to an increasingly challenging series of model problems, and their accuracy is examined. The models involve one light and one heavy degree of freedom, and exhibit substantial nonadiabatic behavior. In all of the models the coupling between the light and heavy particles is linear (harmonic). In addition, different external potentials are applied to the heavy particle only. The energies of the light particle quantum states, as a function of the position of the heavy particle, define a sequence of ground and excited Born–Oppenheimer potential energy curves. Because the light particle experiences a purely harmonic potential, the potential energy curves are parallel and equally spaced for all of the models. In addition, the nonadiabatic couplings among potential energy curves persist for all times due to the nonvanishing linear coupling between light and heavy particles. The model problems were used to test two strategies for carrying out mixed quantum-classical dynamics in systems involving nonadiabatic transitions: mean field and surface hopping. The model calculations reported here suggest that, in cases where linear couplings dominate, the mean field mixed quantum-classical method displays useful accuracy and is robust to the introduction of anharmonic heavy-particle interactions. The model calculations also reveal special situations in which the surface hopping approximation is inappropriate. © *1998 American Institute of Physics.* [S0021-9606(98)52436-1]

I. INTRODUCTION

Many dynamical phenomena in physics and chemistry involve coupled motions of particles with widely differing masses. Electronic and nuclear degrees of freedom, respectively, in single atoms and molecules, provide a vivid illustration, which the Born–Oppenheimer separation scheme[1] exploits to a good advantage. The transfer of light protons along hydrogen bonds between pairs of heavy electronegative atoms (e.g., N, O, F, Cl) constitutes another class of examples.[2] The interaction of liquid ^{3}He or ^{4}He with high-atomic-weight solids, both crystalline and amorphous, presents further illustrations.[3]

The presence of extreme mass ratios invites the use of a mixed quantum and classical description.[4] This is particularly appropriate for describing the (virtually classical) motions of electron-bearing heavy atoms or molecules that form nonreactive insulating media. That is precisely the basis of the molecular dynamics simulation method, for which the Born–Oppenheimer ground-electronic-state energy surface provides the potential energy function for numerical integration of Newton's equations.[5,6] Assuming that electronic excitation remains absent, methods are available when required to generate quantum corrections to the strict classical dynamical description of the heavier particles.[7–10] On the other hand, there are methods that can accurately treat the electron dynamics even if electronic excitations occur but provided that their impact on the motion of the heavier atoms is negligible.[11–14]

Difficulties begin to arise in those cases where electronic (or other light particle) excitations out of the ground state become significant and these, in turn, influence the behavior of the heavier particles. One encounters this situation, for example, in photochemical reactions involving nonradiative transitions, and in oxidation-reduction or proton transfer reactions in liquid solutions. Accurate description of structure and dynamics in liquid metals and reactions at metal surfaces are also problematic, since a continuum of excited conduction electrons must be involved.

The intrinsic power of molecular dynamics computer simulations to illuminate physical and chemical phenomena has lent considerable weight to extending its traditional classical version as described above, to cover cases with electronic excitation. Indeed several approximation schemes for realizing this goal treating the quantum and classical degrees of freedom self-consistently have been proposed (for reviews, see Refs. 15 and 16). These include both mean field[17–33] and surface hopping[34–42] approaches. But in spite of an extended effort no universally acceptable approximation strategy has yet emerged. The present paper reports results of a modest study intended to contribute some further understanding to this active research area. In particular, our

[a)]Current address: Department of Chemistry, University of California, Irvine, Irvine, California 92697.

efforts could be regarded as an attempt to understand to what degree the use of some of these methods is appropriate when the evolution of a heavy plus light particle system is studied using the particle coordinates directly (rather than some collective coordinates). For simple model problems it would be more appropriate to base a quantum-classical separation on normal mode coordinates in order to minimize the effect of the quantum coordinates on the classical ones, and vice versa. In realistic many particle simulations a normal mode separation is not practical, however, and the bare particle must generally be used. This introduces coupling between classical and quantum coordinates, even in harmonic systems, and this coupling can be problematical for mixed quantum-classical dynamics. The simplest model potentials that represent this situation are those of linearly coupled harmonic and anharmonic oscillators. In this context nonadiabatic transitions may occur between the adiabatic (Born–Oppenheimer) light-mass states simply because the bare particle coordinates do not correspond to the ''normal modes'' of the system. The following section argues in favor of studying simple tractable models of nonadiabatic effects, and introduces three such models, each involving a coupled pair of particles moving in one dimension under the influence of an external potential. Section III provides computational details about the respective dynamical investigations for each of these three models. Section IV presents our numerical results for the three. The final Sec. V discusses the implications of our results for future theoretical and simulational activity.

II. SIMPLE MODELS

Each of the three cases to be examined involves a pair of spinless particles confined to move in one dimension only. The lighter particle of the pair (mass m, position x, momentum p) interacts with the heavier particle (mass M, position X, momentum P) via potential $v(x,X)$. At the same time the heavier particle experiences an external potential $V(X)$. The two-particle Hamiltonian consequently has the form

$$H=\frac{p^2}{2m}+\frac{P^2}{2M}+v(x,X)+V(X). \tag{1}$$

The three cases to be analyzed are distinguished by the corresponding assignments of v and V, to be specified below.

Reliance on one-dimensional models to illuminate three-dimensional phenomena obviously must be viewed with caution. Nevertheless this strategy offers some advantages. In particular, some one-dimensional models can be solved analytically in closed form (see model I below), while others that are not fully solvable may still permit a more thorough analysis than do their more complicated three-dimensions counterparts. Furthermore, various contributing effects in one dimension can usually be easily isolated from model to model, thereby simplifying the task of interpretation. We view the study of nonadiabatic effects in the one-dimensional context as a helpful precursor to the development of theoretical techniques that are broadly applicable to three-dimensional systems.

Let $\psi_n(x,X)$ and E_n be the exact eigenfunctions and eigenvalues for the time-independent wave equation corresponding to the Hamiltonian H in operator form,

$$H\psi_n(x,X)=E_n\psi_n(x,X) \tag{2}$$

subject to given boundary conditions. The general time-dependent solution to this quantum-mechanical problem has the form

$$\Psi(x,X,t)=\sum_n A_n \exp\left[-\frac{i}{\hbar}E_n t\right]\psi_n(x,X) \tag{3}$$

with constant A_n selected to satisfy initial conditions. One must keep in mind that this last equation must be modified to include an appropriate integral over continuum states when they exist for a case under consideration.

The Born–Oppenheimer (BO) approximation replaces the full quantum problem Eq. (2) by a sequential pair of single-particle problems. The first examines the light particle motion in the presence of a stationary heavy particle (i.e., fixed at position X),

$$H^{(0)}(x|X)\,\phi_j(x|X)=\epsilon_j^{(0)}(X)\,\phi_j(x|X), \tag{4}$$

where $H^{(0)}(x|X)$ simply contains X as a parameter,

$$H^{(0)}(x|X)=\frac{p^2}{2m}+v(x,X). \tag{5}$$

The second utilizes $\epsilon_j^{(0)}(X)$ as a supplement to $V(X)$ for motion of the heavy particle,

$$H_j^{(1)}(X)\,\varphi_{l,j}(X)=\epsilon_{l,j}^{(1)}\varphi_{l,j}(X), \tag{6}$$

where now

$$H_j^{(1)}(X)=\frac{P^2}{2M}+V(X)+\epsilon_j^{(0)}(X). \tag{7}$$

The outcomes of this sequential approximation are estimates for the exact eigenfunctions

$$\psi_n(x,X)\approx\phi_j(x|X)\,\varphi_{l,j}(X) \tag{8}$$

and for the exact eigenvalues

$$E_n\approx\epsilon_{l,j}^{(1)} \tag{9}$$

for the full two-particle Hamiltonian H. In principle these estimates could be inserted into Eq. (3) to approximate time dependence of the two-particle dynamics.

For all three models to be examined, the interaction $v(x,X)$ was assumed to depend only on relative separation $x-X$, and in particular was chosen to be harmonic,

$$v(x,X)=\tfrac{1}{2}k(x-X)^2. \tag{10}$$

Consequently the light and heavy particles are bound together, forming a kind of ''harmonic hydrogen atom.'' As a result of this extra simplification, the first stage of the BO sequential approximation, Eqs. (4)–(5), leads to the explicit results[43]

$$\phi_j(x|X)=N_j \exp[-\tfrac{1}{2}s^2]H_j(s), \tag{11}$$

$$\epsilon_j^{(0)}=(j+\tfrac{1}{2})\hbar\omega^{(0)}, \tag{12}$$

where H_j is the Hermite polynomial, N_j is the normalization constant,

$$s=(mk/\hbar^2)^{1/4}(x-X), \tag{13}$$

and $\omega^{(0)}$ is the harmonic frequency for the light particle oscillating about the fixed heavy particle, $\omega^{(0)}=(k/m)^{1/2}$. Note that m is larger than the reduced mass for the pair of particles, $\mu=mM/(m+M)$; consequently $\omega^{(0)}$ is smaller than $\omega=(k/\mu)^{1/2}$, the natural oscillation frequency for the pair in free space.

Our three models are now distinguished by the following $V(X)$ choices:

$$\begin{aligned} &V(X)=\tfrac{1}{2}KX^2, \quad \text{model I,}\\ &V(X)=\epsilon[\exp(-2\alpha X)-2\exp(-\alpha X)], \quad \text{model II,}\\ &V(X)=AX^4+BX^2, \quad \text{model III.}\end{aligned} \tag{14}$$

The first is fully harmonic, and therefore fully solvable by separation into independent normal modes. The second involves a Morse oscillator potential for the heavy particle, and can be viewed as a one-dimensional analog of an atom-substrate binding potential of the type often encountered in surface physics and chemistry.[44] The third introduces quartic anharmonicity, and if $A>0$, $B<0$ it can represent bistable motion.

Because the $\epsilon^{(0)}$, Eq. (12), are equally spaced and independent of X for the harmonic v choice, Eq. (10), the adiabatic potential surfaces for motion of the heavy particle are parallel and equally spaced for all three models. Note that sets of parallel potentials also originate when the system is chosen such that in the diabatic representation it is a tridiagonal Hamiltonian matrix where all the diagonal terms are identical functions of the classical coordinates and the off-diagonal couplings are properly chosen constants, all independent of the classical subsystem coordinate.

III. SOLUTION PROCEDURE

Our objective for each of the three models is to determine the precise quantum evolution of an initial wave packet state, and to compare these results with predictions of two specific approximation schemes (Ehrenfest mean field[17–33] and fewest switches surface hopping[35]).

The initial state is selected to conform to the BO ''picture'' reflecting the intention to use the heavy and light particle coordinates as the relevant coordinates. For the model potentials that are explored below the use of approximately separable linear combinations of the bare coordinates might simplify our efforts. But despite this possibility this alternative was rejected in order to retain generality, given that as the complexity of the system increases it becomes more difficult to identify such combinations. In particular, the light particle is placed in one of the $H^{(0)}$ eigenstates, ϕ_j, and the heavy particle in a translating Gaussian wave packet. Consequently, we set

$$\Psi(x,X,t=0)=N\phi_j(x|X)\exp\left[-\frac{i}{\hbar}k_0X-\frac{(X-X_0)^2}{\sigma^2}\right]. \tag{15}$$

Here N is a normalizing constant, X_0 the initial mean position of the heavy particle, $-\hbar k_0$ is the initial momentum, and the width parameter σ is assigned values typically around 20 times the inverse of the initial momentum, unless otherwise noted. The BO functions $\phi_j\varphi_{l,j}$ form a complete set for all three models, and could be used for propagation in time. Indeed one of our objectives is to monitor time dependence of the light particle quantum-state probabilities

$$a_i(t)=\sum_j c^*_{j,i}(t)c_{j,i}(t), \tag{16}$$

where

$$c_{j,i}(t)=\int dX\,\varphi^*_{j,i}(X)\int dx\,\phi^*_i(x|X)\Psi(x,X,t) \tag{17}$$

that indicate transitions between the adiabatic potential surfaces. In addition to following the $a_i(t)$ we have found it useful to examine the time dependence of the heavy particle mean position and momentum,

$$\langle X\rangle(t)=\int\int dx\,dX\;\Psi^*(t)X\Psi(t), \tag{18}$$

$$\langle P\rangle(t)=\int\int dx\,dX\;\Psi^*(t)P\Psi(t). \tag{19}$$

We present these results below as phase space diagrams, i.e., as curves in the X, P plane.

Model I has the advantage that the fully quantum problem is solvable in terms of independent normal modes (see Appendix). This is used when examining the system time evolution. First, the trivial time evolution in the normal modes basis set is calculated and then transformed into the BO basis set to obtain the a_i mentioned above. Note that these normal mode quantum states differ from the BO states by an amount dependent on the mass ratio m/M; as the ratio goes to zero the two representations converge to one another. However when the ratio is nonzero the chosen initial state [Eq. (15)] cannot be a proper normal mode eigenstate, so that the subsequent evolution inevitably involves transitions between the BO surfaces. Therefore this model is a very simple case to study the extent to which the mixed quantum-classical approximation schemes under consideration are suitable to represent the system evolution using the particle coordinates explicitly.

To calculate the full quantum evolution for models II and III fast Fourier transform techniques are used. The procedure used to solve the two-dimensional time dependent Schrödinger equation is that of Kosloff and Kosloff[45] generalized to n light particle states (the n accessible adiabatic states). To do so $\Psi(x,X,t)$ is expanded in the $\phi_j(x|X)$ basis; it becomes

$$\Psi(x,X,t)\rightarrow\begin{pmatrix}\Theta_0(X,t)\\ \Theta_1(X,t)\\ \Theta_2(X,t)\\ \cdots\\ \Theta_n(X,t)\end{pmatrix}, \tag{20}$$

where

$$\Theta_i(X,t)=\int dx\,\phi_i^*(x|X)\Psi(x,X,t) \tag{21}$$

is a wave function evolving on $V_i(X)=V(X)+\epsilon_i^{(0)}(X)$, and the Hamiltonian becomes a nondiagonal matrix,

$$\mathscr{H}_{i,j}(X)=\int dx\,\phi_i^*(x|X)H(x,X)\phi_j(x|X). \tag{22}$$

Thus the two-dimensional time evolution problem has been transformed into n-coupled one-dimensional time dependent Schrödinger equation. Note that the coupling occurs because the BO basis functions, $\phi_j(x|X)$, are not eigenvectors of the P operator included in H [see Eq. (1)]. As the m/M ratio goes to zero the coupling vanishes, and as in the case of model I transitions cease to occur.

The precise full quantum results will be compared with results generated by the two approximate methods mentioned above, Ehrenfest mean field and the fewest switches surface hopping. These are two well-established approximation schemes that are designed to take advantage of the simplicity of classical dynamics for the heavier particle, while presuming to account for nonadiabatic quantum effects of the lighter particle in a self-consistent manner. These methods are described below.

The Ehrenfest mean field approximation postulates classical dynamics for the heavier particle, subjected to an effective force $F_{\rm eff}$ defined as

$$F_{\rm eff}=-\frac{\partial}{\partial X}\left\{V+\int dx\,\Phi^*H^{(0)}\Phi\right\}, \tag{23}$$

where $\Phi(x|X[t])$, the light particle wave function in the presence of the classically moving heavy particle, evolves according to the following time dependent Schrödinger equation,

$$i\hbar\frac{\partial}{\partial t}\Phi(x|X[t])=H^{(0)}(x,X[t])\Phi(x|X[t]). \tag{24}$$

These equations define the method and can be used directly. Alternatively the time-dependent solution for the motion of the light particle can formally be expressed

$$\Phi(x|X[t])=\sum_j c_j(t)\phi_j(x|X), \tag{25}$$

using the previously introduced light particle BO basis functions, $\phi_j(x|X)$. These c_j's are the coefficients that will be use to compute the light particle quantum-state probabilities that will be compared with the results of the fully quantum calculations. Clearly, the equations for the c_j's time evolution can be obtained using Eq. (24),

$$i\hbar\dot{c}_j=\epsilon_j^{(0)}c_j-i\hbar\dot{X}\sum_k d_{j,k}c_k, \tag{26}$$

where the dot represents a time derivative and

$$d_{j,i}=\int dx\,\phi_j\frac{\partial\phi_i}{\partial X}. \tag{27}$$

It can be shown, based on conservation of energy arguments, that the effective force is then given by the following expression:

$$F_{\rm eff}=-\frac{\partial V}{\partial X}-\sum_j|c_j|^2\frac{\partial\epsilon_j^{(0)}}{\partial X}-\frac{\epsilon_j^{(0)}}{\dot{X}}\sum_j\frac{\partial|c_j|^2}{\partial t} \tag{28}$$

$$=-\frac{\partial V}{\partial X}-\sum_j|c_j|^2\frac{\partial\epsilon_j^{(0)}}{\partial X}+\sum_{j,l<j}[c_j^*c_l+c_l^*c_j][\epsilon_j^{(0)}-\epsilon_l^{(0)}]d_{j,l}. \tag{29}$$

The first term on the right-hand side in this last equation is the force due to the external potential acting directly on the heavy particle, the second is an adiabatic contribution to $F_{\rm eff}$, while the third term comprises nonadiabatic effects (light particle quantum number changes). Observe that the effective force interpolates among the forces defined separately on each of the accessible states.

Fewest switches surface hopping is an intrinsically stochastic method in which the heavier particle executes finite-time-interval classical motion on distinct surfaces. Equation (26), the time dependent Schrödinger equation for the light particle $\Phi(x|X[t])$ in terms of the light particle adiabatic basis set, is also used here, but the motion of the classical heavy particle evolves on only *one* adiabatic potential surface at each instant of time, with instantaneous ''hopping'' between states according to the fewest switches algorithm. Thus, in contrast to the method described above, the heavier particle is subjected to a force that is simply

$$F=-\frac{\partial}{\partial X}\{V+\epsilon_j^{(0)}\} \tag{30}$$

except for occasional delta-function impulses required to conserve total energy when hops occur. Note that this method, unlike the mean-field method, is defined upon a basis set which in this case is chosen to be the light particle adiabatic basis set, $\phi_j(x|X)$. The fewest switches algorithm minimizes the number of state switches while maintaining a statistical distribution in an ensemble of trajectories that closely reproduces the light particle state populations. To do so, instantaneous switching probabilities from the occupied level i to all the others states j during the time interval t to $t+\Delta$ are calculated as

$$g_{k,j}=\frac{\Delta b_{j,k}}{|c_k|^2}, \tag{31}$$

where b is defined by [see Eq. (26)]

$$\frac{\partial|c_j|^2}{\partial t}=\sum_{k\neq j}b_{j,k} \tag{32}$$

$$=-2\dot{X}\sum_{k\neq j}\mathrm{Re}[c_j^*c_kd_{j,k}], \tag{33}$$

and compared to a uniform random number, ξ between 0 and 1 to determine if a switch is to occur. For example, if $j=1$, a switch to state 2 will occur if $\xi<g_{1,2}$. A switch to state 3 will occur if $g_{1,2}<\xi<g_{1,2}+g_{1,3}$, etc. In addition, for a hop to occur the kinetic energy of the classical particle must be large enough to compensate for the loss in potential energy that might be involved in the transition. To understand how the algorithm works note that if the system has only two levels the switching probability is the rate at which the quantum light particle population probability is increasing on the surface where the classical particle might hop. In the absence of ''forbidden'' hops, i.e., the appearance of nonzero amplitudes in states that are energy forbidden, the fewest switches algorithm statistically partitions trajectories correctly among different potential energy surfaces according to the probabilities $|c_j|^2$. The treatment of forbidden hops is discussed below.

The approximate mixed quantum-classical methods involve solving both the time dependent Schrödinger equation (26) and the Newton equations. Both were solved numerically using the Runga–Kutta–Gill method.[46]

IV. NUMERICAL RESULTS

A. Model I: Harmonic oscillator

This model consists of harmonic potentials in both the heavier and lighter particle coordinates, with a coupling that could be viewed as bilinear [expanding the square of $(x-X)$],

$$H(x,X)=\frac{p^2}{2m}+\frac{P^2}{2M}+\frac{1}{2}\,k(x-X)^2+\frac{1}{2}\,KX^2. \tag{34}$$

In this section some representative results for this model will be described.

As mentioned above the evolution of a system under this Hamiltonian can be determined trivially by transforming the problem into its separable (normal) modes, see Appendix. This will be used to calculate the exact (fully quantum) evolution of the system. But we reiterate that the motions of the heavy and light particles will be viewed as such, drawing upon the Born–Oppenheimer representation. Figure 1(a) displays the potential surfaces, the BO eigenvalues plus the heavy particle external potential [see Eq. (12)],

$$V_n(X)=\tfrac{1}{2}\,KX^2+(n+\tfrac{1}{2})\hbar\sqrt{k/m}, \tag{35}$$

$$V_n(X)=\tfrac{1}{2}\,15X^2+(n+\tfrac{1}{2})\sqrt{5}. \tag{36}$$

These equations indicate choices for some of the parameters used in our numerical calculations. In addition the masses $m=1$ and $M=10$ were assigned, and for convenience we use atomic units. The width parameter was chosen to be $\sigma=0.15$ in Eq. (15) and is such that the results do not significantly change when σ is smaller. Initially the ground state is the only populated adiabatic state, and X_0 and $-\hbar k_0$ [the large dot in the Fig. 1(a)] are the initial conditions of the heavy particle in the mixed quantum-classical methods or the center of the wave packet in the fully quantum calculations.

The ratio of masses is such that this example falls clearly in a regime were the BO approximation should not hold and transitions between the levels must occur. The separation of the parallel adiabatic states assures that when a transition occurs the amount of energy transferred from the quantum degree of freedom to the classical one affects the dynamics of the heavy particle. This problem then may represent a challenge to any of the approximation methods.

First we concentrate on the mean field approximation. Figure 1(b) shows the phase space diagram. The solid line corresponds to the solution of the fully quantum problem ($\langle X\rangle$ is plotted vs $\langle P\rangle$). The mean field results (X is plotted vs P) are essentially identical to the fully quantum results. The dotted line is the quantum adiabatic approximation solution, i.e., no transitions ($\langle X\rangle$ is plotted vs $\langle P\rangle$). Thus exact quantum and mean field versions are identical, even though as shown by the contrast with the adiabatic approximation, transitions occur to a great extent. This result can be understood with the aid of the Ehrenfest theorem[47] which states that for any Hamiltonian of the form

$$H(q)=\frac{p_q^2}{2m}+V(q), \tag{37}$$

the mean values $\langle q\rangle$ and $\langle p_q\rangle$ are given by

$$\frac{d}{dt}\langle q\rangle=\frac{\langle p_q\rangle}{m};\quad \frac{d}{dt}\langle p_q\rangle=-\left\langle\frac{dV}{dq}\right\rangle. \tag{38}$$

When applied to the present completely harmonic model, Eq. (34), we obtain

$$\frac{d}{dt}\langle x\rangle=\frac{\langle p\rangle}{m};\quad \frac{d}{dt}\langle p\rangle=-k(\langle x\rangle-\langle X\rangle); \tag{39}$$

$$\frac{d}{dt}\langle X\rangle=\frac{\langle P\rangle}{M};\quad \frac{d}{dt}\langle P\rangle=-(k+K)\langle X\rangle-k\langle x\rangle. \tag{40}$$

Alternatively, invoking the mean field approximation for the heavy particle motion, and then taking the classical limit, produces the following Newton equations of motion:

$$\frac{d}{dt}X=\frac{P}{M};\qquad \frac{d}{dt}P=\frac{\partial}{\partial X}\left\{\frac{1}{2}\,KX^2+\int dx\,\Phi^* H^{(0)}\Phi\right\}$$
$$=KX-\int dx\,\Phi^*\left[\frac{\partial H^{(0)}}{\partial X}\right]\Phi$$
$$=-(K+k)X-k\langle x\rangle, \tag{41}$$

where the fact that Φ is the solution of the time dependent Schrödinger equation involving $H^{(0)}$ has been applied to obtain the second to the last equation. The dynamics of the quantum degree of freedom can be examined applying the Ehrenfest theorem to $H^{(0)}$ [see Eq. (4)], this leads to

$$\frac{d}{dt}\langle x\rangle=\frac{\langle p\rangle}{m};\ \frac{d}{dt}\langle p\rangle=-k(\langle x\rangle-X), \tag{42}$$

where here as in the rest of the paper the $\langle\,\rangle$ represents integration over the quantum degree(s) of freedom. Note how the equations of motion, Eqs. (41) and (42), are identical to the solution of the fully quantum problem, Eqs. (39) and (40) (with $X\leftrightarrow\langle X\rangle$ and $P\leftrightarrow\langle P\rangle$), explaining why the mean field approximation is exact while calculating the evolution of the heavy particle. This is true only because the coupling is bi-

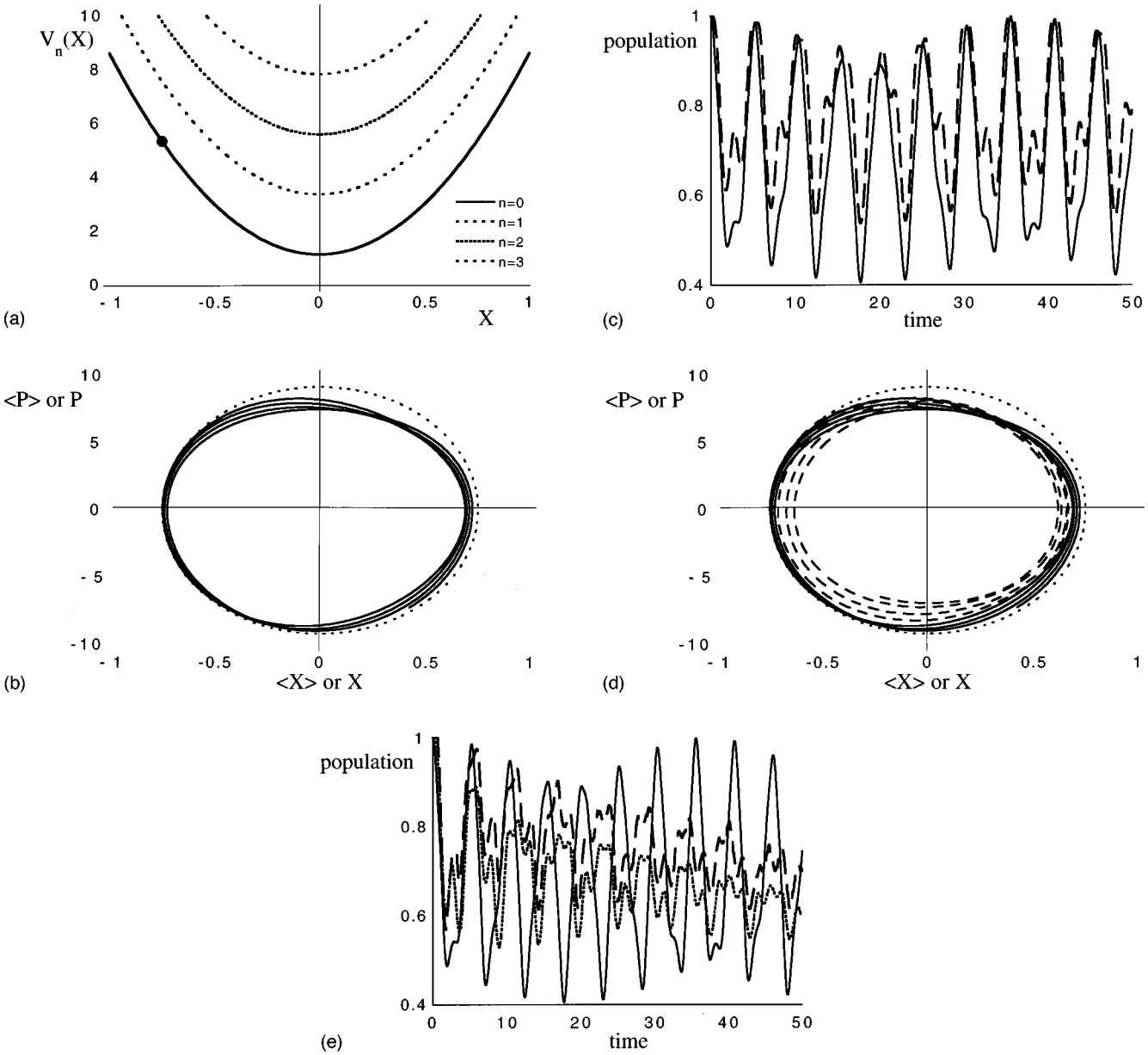

FIG. 1. Numerical example for model I: Harmonic oscillator. (a) Potential surfaces. The small circle indicates the initial position of the heavy particle (in the mixed quantum-classical calculations) or the center of the wave packet (in the fully quantum calculations). (b) Mean field results: Phase space diagram. The solid line corresponds to the solution of the fully quantum problem ($\langle X\rangle$ is plotted vs $\langle P\rangle$). For this case the *mean field* results (X vs P) are identical to the fully quantum results. The dotted line corresponds to the quantum adiabatic approximation solution ($\langle X\rangle$ is plotted vs $\langle P\rangle$). The figure shows the first 20 time units of the evolution. (c) Mean field results: Evolution of populations. The solid line is the numerically exact ground state population and the broken line is the result of the *mean field* approximation, both are plotted as a function of time. Only the ground state population is shown for clarity although there is population transfer to the first and second excited states. (d) Surface hopping results: Phase space diagram. The solid line corresponds to the solution of the fully quantum problem, the broken line to the *surface hopping* results (average X is plotted vs average P) and the dotted line to the quantum adiabatic approximation solution. The first 20 time units of the evolution are shown. (e) Surface hopping results: Evolution of populations. The solid line is the numerically exact ground state population, the broken line the population calculated as the fraction of trajectories on each surface and the dotted line the population calculated as the average (over all the different trajectories) of $|c_i|^2$. The last two are results of the *surface hopping* approximation. As in (c) only the ground state population is shown for clarity.

linear and the potentials quadratic in both coordinates, otherwise deviations occur as will be seen below. As a curiosity (it is hard to envision a practical direct use of what follows) note that if the role of x and X are interchanged while applying the mean field method (the heavier particle is treated by quantum mechanics and the lighter by classical mechanics) their evolution in phase space would still be described exactly.

Even for harmonic models, the mean-field mixed quantum-classical method is exact only in reproducing the first moments, $\langle X\rangle$ and $\langle P\rangle$. Higher moments are not computed exactly. This is apparent when comparing the time dependence of the light particle quantum-state probabilities in Fig. 1(c). While the curves resemble each other, they are not identical.

Overall the performance of the mean field method is remarkably good for model I. The harmonic oscillator problem is peculiar and therefore it is interesting to study to what

degree this result survives when the harmonicity is somehow relaxed. Clearly, there are circumstances where the method will eventually stop performing well. In particular, as has been described in detail elsewhere[15,35,42,48] this method cannot describe accurately the evolution of minority reaction channels if these channels involve potential energy surfaces that differ considerably from the one experienced by the majority channel. Note that this is precisely the class of problems that the method of surface hopping was designed to address.[35] It would be of little use to modify the potential just in order to see the mean field approximation fail; it seems more informative instead to concentrate on a specific class of potentials. Here, as mentioned earlier, we will focus on the class of potentials that are harmonic in the separation between x and X but let the $V(X)$ change (the potential energy surfaces are then constrained to be parallel) and monitor the degree to which the given approximation holds.

Now we focus on the performance of the second approximation method, the fewest switches surface hopping algorithm. The results shown correspond to averaging 1000 trajectories, all starting at $(X_0, -k_0\hbar)$ but with a different stochastic history of hops. Figure 1(d) shows the resulting phase space diagrams. The different lines have a similar meaning to those in Fig. 1(b) although here the classical quantities represent an average over all the trajectories. Note how the first two curves differ significantly, especially at longer times. Figure 1(e) shows the population evolutions. The solid line is the exact result, the broken line the population calculated as the fraction of trajectories on each surface, and the dotted line the population calculated as the average (over all the different trajectories) of $c_i^* c_i$. At early times, the populations computed by surface-hopping are very similar to the mean field results of Fig. 1(c). At longer times, the results of surface hopping show damped oscillations in the populations and an inward spiraling in the phase space diagram. This can be attributed to the fact that different trajectories exhibit a different history of random hops. Over a period of time this causes the ensemble to lose coherence and therefore spread in phase space. A second factor that can introduce error in surface hopping is associated with ''forbidden hops.'' With the algorithm employed here, hops induced by the evolving quantum populations are tested for energetic feasibility. In the present calculation the classical particles were started at a turning point and immediately quantum population began to develop on the upper surface. On the other hand some time elapses before the classical particle reaches a position where it is energetically possible for it to begin to evolve on the upper energy surface. As a consequence the fewest switches algorithm fails to statistically partition trajectories correctly among different potential energy surfaces. This will not appear to be the major source of error in this case, however.

A related issue is that of the treatment of a forbidden surface hop. It has been argued[49] that the velocity of the classical particle should be reversed after such an occurrence. More recently, Müller and Stock[48] have shown that it may be more accurate to continue motion in the same direction.

The reason behind the unsatisfactory performance of the surface hopping algorithm for longer times is not related to the precise nature of the potential in model I. Whenever the potential involves a coupling that does not vanish outside a localized scattering region, surface hopping will introduce unphysical loss of coherence. In addition, this class of interactions also encourages the presence of regions where the hops are classically forbidden but encouraged by quantum mechanics. This situation describes all of the models studied in this work; they involve heavy and light particles connected by a spring and therefore coupled for all times. The only difference between them is the profile of the scattering region. This fact plus the explicit exclusion (see earlier) of the class of potentials were the surface hopping method is known to outperform the mean field method motivates us to focus on the performance of the mean field approximation.

B. Model II: Morse oscillator A

In relaxing the harmonic restriction in the form of $V(X)$ an obvious choice is that of the Morse oscillator,

$$H(x,X) = \frac{p^2}{2m} + \frac{P^2}{2M} + \frac{1}{2}\,k(x-X)^2 + \epsilon[\exp(-2\alpha X) - 2\exp(-\alpha X)]. \tag{43}$$

In this section some representative results for this model will be described. Figure 2(a) displays the potential surfaces,

$$V_n(X) = \epsilon[\exp(-2\alpha X) - 2\exp(-\alpha X)] + (n+\tfrac{1}{2})\hbar\sqrt{k/m}, \tag{44}$$

$$V_n(X) = 60[\exp(-0.6X) - 2\exp(-0.3X)] + (n+\tfrac{1}{2})\sqrt{200}. \tag{45}$$

Also shown in the equation above is the choice of some of the parameters used in this calculation. As before, the masses are $m=1$ and $M=10$, and initially the ground adiabatic state is the only one populated in the lighter particle degree of freedom.

The anharmonicity of the potential causes the quantum wave packet to deform, losing its Gaussian shape as time progresses, unlike model I. Therefore, when using this mixed quantum-classical method one trajectory is not sufficient. It is necessary to perform dynamics for a collection of trajectories differing in the initial position and momentum of the heavy particle. To choose the initial conditions we have used a Wigner transform.[50] The Wigner transform carries a density operator in the coordinate representation $\rho(X,X') = |\Theta(X)\rangle\langle\Theta(X')|$ to phase space;

$$\rho(X,P) = \frac{1}{\pi\hbar}\int_{-\infty}^{\infty} dY \langle X-Y|\rho(X,X')|X+Y\rangle \times \exp[2iPY/\hbar]. \tag{46}$$

From this $\rho(X,P)$ the set of different initial conditions for the collection of trajectories is chosen. The number of different initial conditions is such that the results are substantially independent of it, and this number depends not only on the potential surface but also on the initial conditions and length of the dynamics.

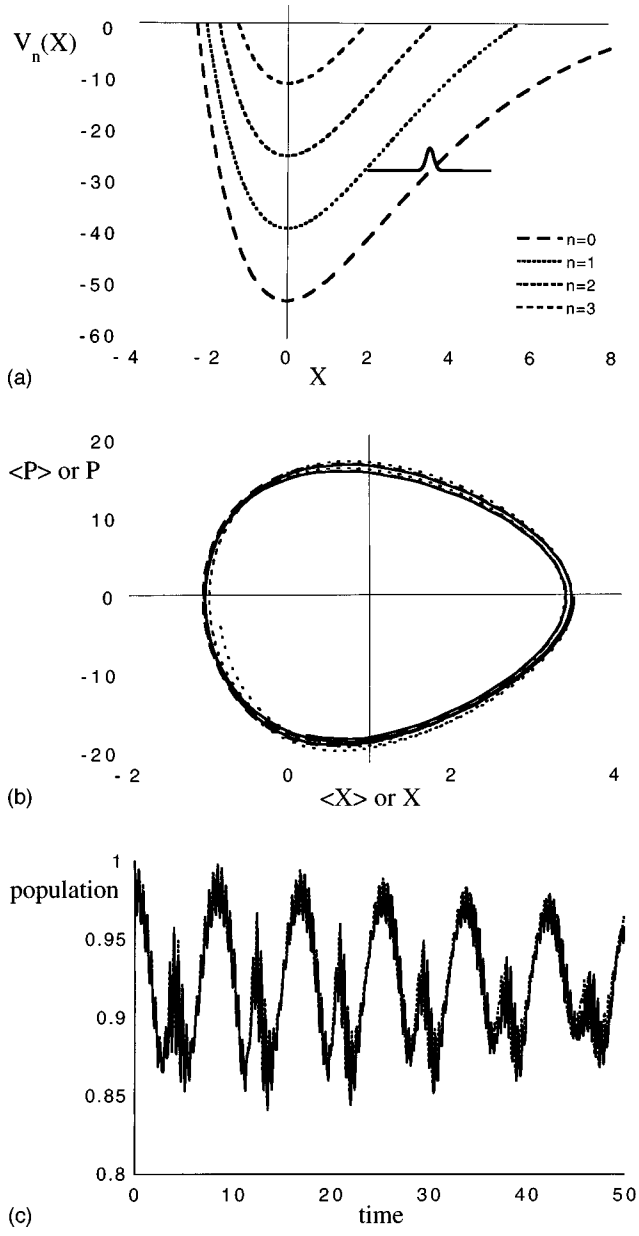

FIG. 2. Numerical example for model II: Morse potential A. (a) Potential surfaces. The initial wave packet, $\Theta_0(X,t=0)$ (see text), is also shown. (b) Phase space diagram. The solid line corresponds to the solution of the fully quantum problem ($\langle X\rangle$ is plotted vs $\langle P\rangle$), the broken line to the *mean field* results (ensemble averaged X vs ensemble averaged P) and the dotted line to the quantum adiabatic approximation solution ($\langle X\rangle$ is plotted vs $\langle P\rangle$). The figure shows the first 20 time units of the evolution. (c) Evolution of populations. The solid lines are the numerically exact populations and the broken lines are the result of the ensemble averaged *mean field* approximation, both are plotted as a function of time. Only the ground state population is shown for clarity although there is population transfer to the first and second excited states.

Figure 2(b) shows phase space diagrams. The solid line corresponds to the solution of the fully quantum problem (solved numerically as described in Sec. III), the broken line to the ensemble averaged mean field results and the dotted line to the quantum adiabatic approximation solution. Figure 2(c) shows the time dependence of the light particle quantum-state probabilities. Even though the results are not identical, the method performance is still quite good. We emphasize that this result, although representative, was obtained keeping in mind the goal of finding the limitations of the mean field method for this class of potentials. Its success motivated the selection of model III described in the next subsection.

C. Model III: Double well

The mean field method cannot properly describe situations for which the wave packet bifurcates into two or more distinct paths governed by different interactions.

Model III introduces quadratic anharmonicity that can represent bistable motion (if $A>0$ and $B<0$),

$$H(x,X)=\frac{p^2}{2m}+\frac{P^2}{2M}+\frac{1}{2}\,k(x-X)^2+AX^4+BX^2. \quad (47)$$

In what follows some representative results for this model will be described, and again the conditions were chosen as to maximize the chances of the mean field method to fail. Figure 3(a) displays the potential surfaces,

$$V_n(X)=AX^4+BX^2+(n+\tfrac{1}{2})\hbar\sqrt{k/m}, \quad (48)$$

$$V_n(X)=X^4-12X^2+(n+\tfrac{1}{2})\sqrt{300}, \quad (49)$$

that are accessible. As in the previous models, the masses are $m=1$ and $M=10$. The initial state is the ground adiabatic state in the lighter particle degree of freedom; and the heavier particle degree of freedom is a Gaussian wave packet in the fully quantum calculation, while in the mixed classical-quantum calculations it is described by a collection of X_0 and $-\hbar k_0$ (the initial conditions for the set of trajectories) chosen from a Wigner distribution as described in the previous subsection.

Figure 3(b) shows phase space diagrams. The solid line corresponds to the solution of the fully quantum problem (solved numerically as described in Sec. III), the broken line to the ensemble averaged mean field results and the dotted line to the quantum adiabatic approximation solution. Figure 3(c) shows the time dependence of the light particle quantum-state probabilities. Note that the phase space trajectory, Fig. 3(b), spirals inwards approaching an unsymmetric position of x about 0.5. Quantum mechanically, this is due to trapping of the fraction of the wave packet that has been excited to the $n=1$ level. The initial conditions of the wave packet have been chosen so that there is sufficient energy for most of the wave packet to traverse the barrier in the ground $(n=0)$ state, but not in the first excited $(n=1)$. Tunneling through the excited state is sufficiently slow that the asymmetry in position persists over the time scale of the calculation. It is interesting to note that the mean field approximation reproduces this effect quite well, at least in an average way. There is a spread of initial energies of the independent mean field trajectories, determined from the Wigner distribution. For the conditions of Fig. 3, trajectories in the low energy tail of this distribution get trapped by the potential barrier (slightly higher that the ground state barrier due to mixing with the excited state). The high energy majority traverse the barrier. The phase space asymmetry in the mean-field result of Fig. 3 is thus largely determined by the width of the initial momentum distributions, not by the probability of excitation to the $n=1$ state as in the fully quantum case.

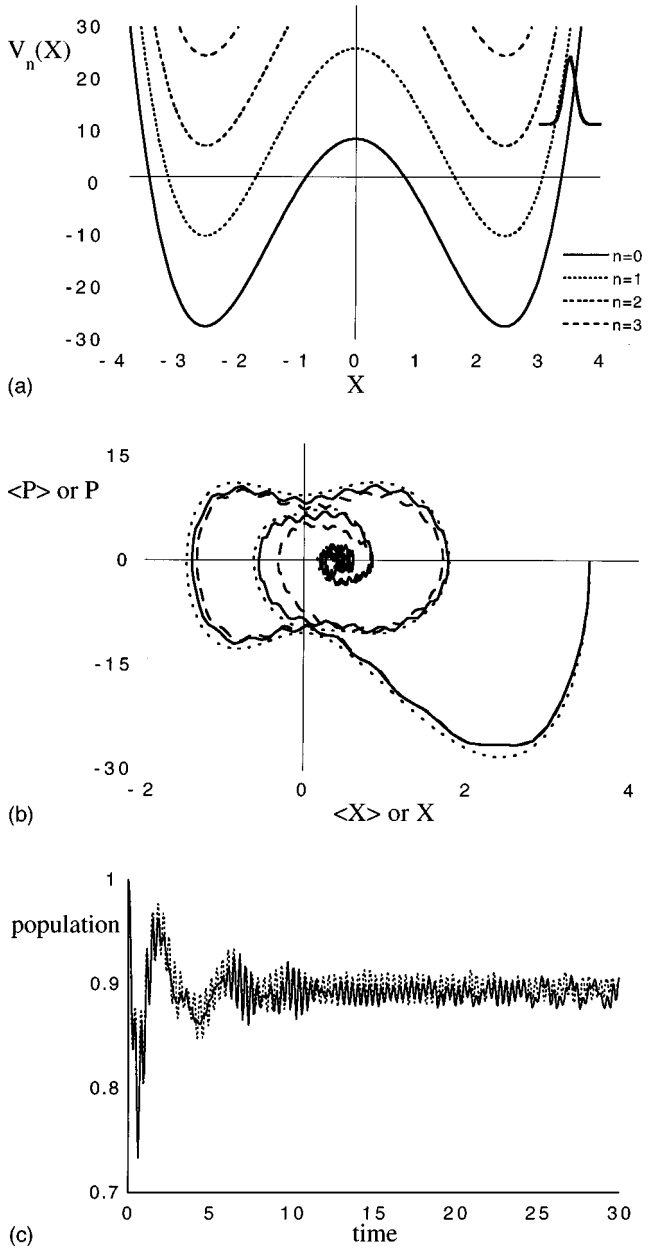

FIG. 3. Numerical example for model III: Double well. (a) Potential surfaces. The initial wave packet, $\Theta_0(X,t=0)$ (see text), is also shown. (b) Phase space diagram. Same as Fig. 2. (c) Evolution of populations. Same as Fig. 2.

Nevertheless, on average, the mean field method quite accurately reproduces the asymmetry of the full quantum calculation, at least for the initial conditions chosen here.

Even though the results are not perfect the performance of the mean field method is still quite good, despite the fact that during the evolution a small but significant portion of the population is in the excited state. Note that at the energy we selected, the potential does not permit exploring large regions of space. This may imply that even when the detailed evolution is not being described properly, the evolution of the averaged quantities that are being measured is accurate. Therefore, in the next section model II will be re-examined but in a case were the evolution is not confined to a restricted region of space.

D. Model II revisited: Morse oscillator B and C

The potential surfaces involved in the first example in this subsection are displayed in Fig. 4(a),

$$V_n(X) = 10[\exp(-1.0X) - 2\exp(-0.5X)] + (n+\tfrac{1}{2})\sqrt{30}. \tag{50}$$

Note that these differ from the case shown above in Eq. (45). The initial conditions were chosen so that a small but non-negligible fraction of population might be transiently trapped in the well of the first excited potential curve. The masses are $m=1$ and $M=10$, and the initial state is the ground adiabatic state in the lighter particle degree of freedom, and in the heavier particle degree of freedom it is a Gaussian wave packet in the fully quantum calculation, and in the mixed classical-quantum calculations it is described by a set of X_0 and $-\hbar k_0$ as already stated. The initial state in the heavier particle degree of freedom, $\Theta_0(X)$, is also shown in Fig. 4(a), its baseline representing total energy of the system in this calculation. Note that outside the well region the total energy is less than $V_1(X)$.

Figure 4(b) shows phase space diagrams. The solid line corresponds to the solution of the fully quantum problem ($\langle X\rangle$ vs $\langle P\rangle$), the broken line to the ensemble averaged mean field results, and the dotted line to the quantum adiabatic approximation solution. Figure 4(c) shows the time dependence of the light particle quantum-state probabilities. Note the persistent oscillations (clearly shown in the inserts displaying the 190–200th time units) in both the populations and in the phase space diagram, resulting from the fact that the coupling between the heavy and light particle does not vanish when the compound particle leaves the scattering region. The oscillations correspond to the periodic transfer of energy between the heavy and light particles, and far from the scattering region simply monitor the behavior of the heavier particle in the unperturbed composite particle.

The amount of population transfer is rather small, despite our efforts to find parameters where the mean field approximation was likely to fail. This surprising situation is caused by the fact that if the initial momentum is increased the size of the oscillations just described increase as well, thus masking any other effects. This adds to the fact that increasing the magnitude of the coupling does not have a significant net effect on the transition rates since k is also proportional to the separation of the levels and therefore inversely proportional to the transition probabilities. Despite this, the method performance is still better than expected even though the populations in the different channels evolve in regions that are quite separated spatially.

This ''puzzle'' can be solved by recognizing that population can be evolving in the upper surface but not be trapped (and therefore not in a minority channel). Figures 4(d) and 4(e) show $\Theta_0(X,t)$ and $\Theta_1(X,t)$, respectively. The region enclosed in the quadrilateral figure in 4(e) is the only portion of the population effectively trapped, and this portion is almost nonexistent. Most of the population in the upper surface behaves as a ''ghost'' of the population on the ground state, the behavior of the former merely mirroring that of the

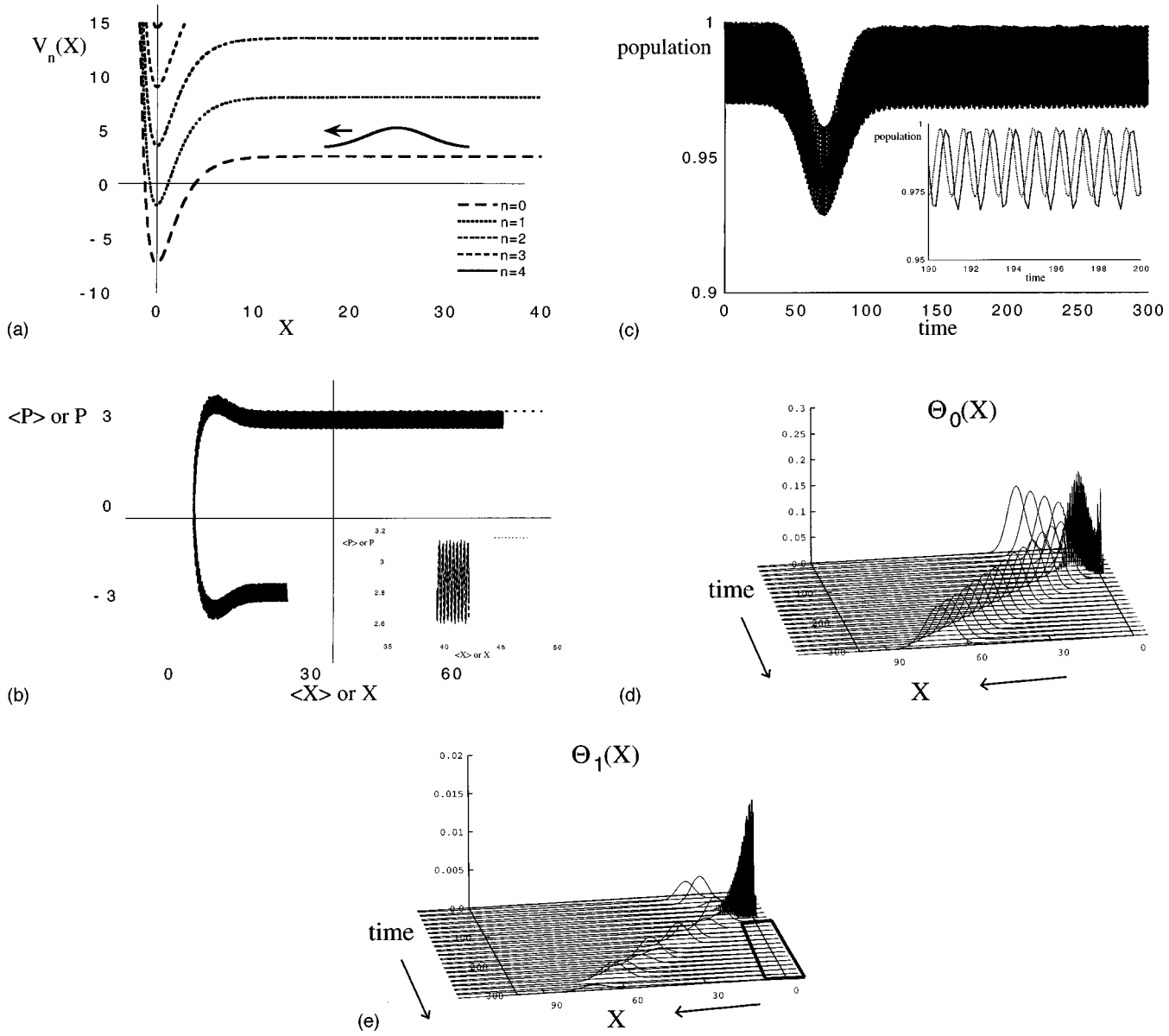

FIG. 4. Numerical example for model II: Morse potential B. (a) Potential surfaces. The initial wave packet, $\Theta_0(X,t=0)$ (see text), is also shown. (b) Phase space diagram. Same as Fig. 2. (c) Evolution of populations. Same as Fig. 2. The inserts in (b) and (c) display the evolution between the 190 and 200 time units. (d) Evolution of $\Theta_0(X,t)$. (e) Evolution of $\Theta_1(X,t)$. The region enclosed in the quadrilateral is the only portion of the population effectively trapped.

latter. This is a consequence of the persistent coupling between the light and heavy particles.

Thus, to observe a significant failure the transition rate must be somehow increased. This may be accomplished by increasing the slope of the inner wall and therefore increasing the match between the frequency of the bounce and that of the oscillations. This creates a small fraction of the population with a significantly different amount of kinetic energy than that of the majority, consequently evolving under inappropriate forces. That is the case if the potential surfaces are

$$V_n(X)=0.001[\exp(-20.0X)-2\exp(-10.0X)] + (n+\tfrac{1}{2})\sqrt{10} \tag{51}$$

as shown in Figs. 5(a)–5(e) (the figures are equivalent to those in Fig. 4). In this example the well is extremely shallow and the inner wall is quite steep; therefore it might represent a collision with a hard wall. To encourage transitions given the absence of a substantial well, the population is initially in the first excited adiabatic state. An alternative would have been to give the heavier particle more initial kinetic energy, but this would have resulted in the appearance of masking oscillations.

This final choice of parameters produces a bifurcation of the initial wave packet into two scattered portions of quite different velocity. An average path cannot be expected to properly describe the individual pathways, so the mean field method is expected to break down. The surface hopping method was developed in order to handle such bifurcation. However, this specific example, in addition to producing a bifurcation, involves a coupling between light and heavy that

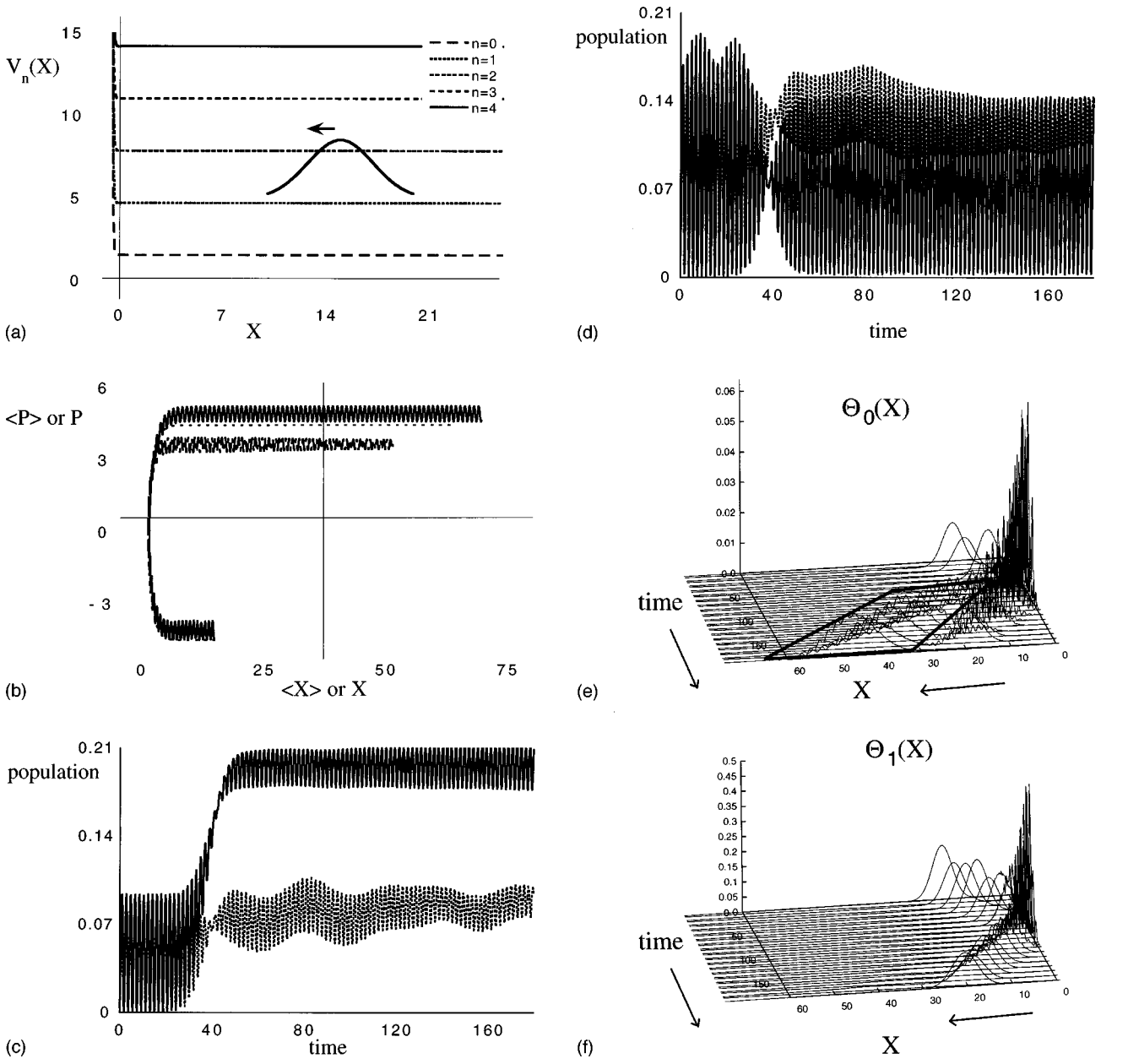

FIG. 5. Numerical example for model II: Morse oscillator C. (a) Potential surfaces. The initial wave packet, $\Theta_1(X,t=0)$ (see text), is also shown. (b) Phase space diagram. Same as in Fig. 2. (c) Evolution of population on the ground state. (d) Evolution of population on the second excited state. Note how when the mean field approximation is used the state to which most of the population is transferred is not the correct one. (e) Evolution of $\Theta_0(X,t)$. The region enclosed in the quadrilateral is the portion of the population evolving in the minority channel. (f) Evolution of $\Theta_1(X,t)$.

never vanishes. It is likely, therefore, that surface-hopping would also have difficulty with this model, at least reproducing the long time oscillatory behavior.

V. DISCUSSION AND CONCLUSIONS

We have examined the accuracy of mixed quantum-classical dynamics as applied to an increasingly challenging series of model problems. The models involve one light and one heavy degree of freedom, and exhibit substantial nonadiabatic behavior. In all of the models the coupling between the light and heavy particles is linear (harmonic). In addition, an external potential is applied to the heavy particle only. The models differ only in the magnitude of the coupling force constant, and the form and magnitude of the external potential. The energies of the light particle quantum states, as a function of the position of the heavy particle, define a sequence of ground and excited Born–Oppenheimer potential energy curves. Because the light particle experiences a purely harmonic potential, the potential energy curves are parallel and equally spaced for all of the models. In addition, the nonadiabatic couplings among potential energy curves persists for all times due to the nonvanishing linear coupling between light and heavy particles.

The model problems were used to test two strategies for carrying out mixed quantum-classical dynamics in systems involving nonadiabatic transitions, mean-field and surface-hopping. With the mean-field approach the classical motion of the heavy particle is governed by an effective potential

energy surface resulting from an average over light particle quantum states, weighted by their time-varying populations. It is well known that this method is inadequate in cases where the quantum wave packet splits into parts that are governed by substantially different forces. The surface-hopping procedure for stochastically splitting a trajectory into multiple branches was developed in order to overcome this difficulty. Surface-hopping has been shown to outperform the mean-field method in such cases.[51] In the present series of model studies, however, the forces associated with each quantum state are identical since the potential energy curves are parallel. The necessity for splitting trajectories into branches is therefore not apparent. Furthermore, the fact that nonadiabatic transitions continue to occur for arbitrarily long times presents a significant obstacle for surface-hopping methods; the different stochastic histories of individual trajectories result in an unphysical loss of quantum coherence at long times. This was demonstrated by application to model I, where surface hopping proved to be an adequate approximation to the exact quantum results at short times, but was inadequate at long times and clearly inferior to the mean field method.

The fact that the forces are identical on each potential energy curve does not ensure the success of the mean-field method. First, the classical approximation is certainly not exactly even when motion is confined to a single potential energy surface. Since our interest here is in mixed quantum-classical treatment of systems involving multiple potential surfaces, we selected model parameters so that classical mechanics provided an accurate description of single surface dynamics, as judged by comparison with exact quantum calculations within the adiabatic approximation. Second, even with parallel potential energy surfaces, the mean-field approximation is not exact. The results reported above help delineate the range of validity of the method.

For a completely harmonic system, model I, we have shown in analogy with the standard Ehrenfest theorem that the mean-field classical heavy particle position X and momentum P reproduce exactly the corresponding quantum mechanical expectation values $\langle X\rangle$ and $\langle P\rangle$. Higher moments of X and P and quantum state probabilities are not reproduced exactly by the mean-field method, but they are quite accurate. With the addition of anharmonicity into the external potential that acts on the heavy particle, models II and III, the Ehrenfest correspondence is no longer exact, and the mean-field results deviate somewhat more from the exact quantum results. Nevertheless, the mean-field method was of acceptable accuracy for all but one of the model systems studied.

For the double well potential, model III, we expected that the mean-field method would be incapable of correctly describing the bifurcation of the quantum wave packet into two parts localized, respectively, in the left and right potential wells. However, the fraction of mean-field trajectories trapped in each well agreed quite accurately with the quantum probabilities as did the mean values of X and P. The only case for which the mean-field method did not provide an acceptable description was the final parameterization of model II, for which the quantum wave packet split into a scattered wave packet on the ground state potential curve and a scattered wave packet on the first excited potential.

The class of models considered here, restricted to linear light–heavy coupling, is admittedly artificial. The models were chosen to elucidate the application of mixed quantum-classical dynamics to condensed phase systems involving many heavy (classical) degrees of freedom which are coupled to a few light (quantum) degrees of freedom. In such systems it is impractical to carry out dynamical simulations using normal mode coordinates. Rather, the bare coordinates of the heavy and light coordinates are generally used. In the bare particle coordinate system, the coupling between light and heavy particles will have a linear term. It is reasonable to suppose that in many cases this linear term will dominate the coupling, particularly when the masses of the light and heavy particles do not differ greatly, e.g., hydrogen versus carbon. The model calculations reported here suggest that, in cases where linear couplings dominate, the mean-field mixed quantum-classical method can be of useful accuracy and is robust to the introduction of anharmonic heavy-particle interactions.

ACKNOWLEDGMENT

We thank Dr. David Sholl for valuable discussions.

APPENDIX: NORMAL MODES OF MODEL I

The total Hamiltonian is

$$H(x,X)=\frac{p^2}{2m}+\frac{P^2}{2M}+\frac{1}{2}k(x-X)^2+\frac{1}{2}KX^2. \tag{A1}$$

If the potential is written in matrix form and in term of mass weighted coordinates $q=\sqrt{m}x$ and $Q=\sqrt{M}X$ it becomes

$$\frac{1}{2}(qQ)\begin{pmatrix}\alpha & \gamma\\ \gamma & \beta\end{pmatrix}\begin{pmatrix}q\\ Q\end{pmatrix}, \tag{A2}$$

where $\alpha=k/m$, $\beta=(k+K)/M$, and $\gamma=-k/\sqrt{mM}$. Therefore to obtain the normal modes it is necessary to solve the following eigenvalue problem:

$$\begin{vmatrix}\alpha-\lambda & \gamma\\ \gamma & \beta-\lambda\end{vmatrix}=0. \tag{A3}$$

The eigenvalues are

$$\lambda_{\pm}=\frac{\alpha+\beta}{2}\pm\sqrt{\frac{(\alpha-\beta)^2}{4}+\gamma^2} \tag{A4}$$

and the corresponding diagonalizing coordinates are

$$\eta=\frac{\gamma}{\mu}q+\frac{(\lambda_+-\alpha)^2}{\mu}Q, \tag{A5}$$

$$\zeta=-\frac{(\lambda_+-\alpha)^2}{\mu}q+\frac{\gamma}{\mu}Q, \tag{A6}$$

where

$$\mu=\sqrt{(\lambda_+-\alpha)^2+\gamma^2}. \tag{A7}$$

The Hamiltonian thus becomes a two-dimensional uncoupled harmonic problem, with normal modes coordinates ζ and η,

$$H(x,X)=\frac{p_\eta^2}{2}+\frac{p_\zeta^2}{2}+\frac{\lambda_+\eta^2}{2}+\frac{\lambda_-\zeta^2}{2} \tag{A8}$$

with solutions

$$\chi_{i,j}(\zeta,\eta)=\xi_i(\zeta)\nu_j(\eta), \tag{A9}$$

$$\nu_j(\eta)=N_j\ \exp[-\tfrac{1}{2}\eta'^2]H_j(\eta'),\quad \epsilon_j^\eta=(j+\tfrac{1}{2})\sqrt{\lambda_+}, \tag{A10}$$

$$\xi_i(\zeta)=N_i\ \exp[-\tfrac{1}{2}\zeta'^2]H_i(\zeta');\quad \epsilon_i^\zeta=(i+\tfrac{1}{2})\sqrt{\lambda_-}, \tag{A11}$$

where $\zeta'=\zeta(\lambda_-/\hbar^2)^{1/4}$, $\eta'=\eta(\lambda_+/\hbar^2)^{1/4}$, H_n are the Hermite polynomials, and N_n are normalization constants.

[1] M. Born and J. R. Oppenheimer, Ann. Phys. (Leipzig) **84**, 457 (1927).
[2] L. Pauling, *The Nature of the Chemical Bond*, 3rd ed. (Cornell University Press, Ithaca, 1960), Chap. 12.
[3] K. R. Atkins, *Liquid Helium* (Cambridge University Press, Cambridge, 1959).
[4] P. J. Rossky and J. Schnitker, J. Phys. Chem. **92**, 4277 (1988).
[5] M. P. Allen and D. J. Tildesley, *Computer Simulation of Liquids* (Clarendon, Oxford, 1987).
[6] L. M. Raff and D. L. Thompson, *Theory of Chemical Reaction Dynamics*, edited by M. Baer (Chemical Rubber, Boca Raton, 1985), Vol. II, p. 1.
[7] E. J. Heller, Acc. Chem. Res. **14**, 368 (1981).
[8] W. H. Miller, J. Chem. Phys. **53**, 1949 (1970).
[9] J. H. Irving and R. W. Zwanzig, J. Chem. Phys. **19**, 1173 (1951).
[10] B. J. Berne and D. Thirumalai, Annu. Rev. Phys. Chem. **37**, 401 (1986).
[11] N. F. Mott, Proc. Cambridge Philos. Soc. **27**, 553 (1931).
[12] E. E. Nikitin, *Theory of Elementary Atomic and Molecular Processes in Gases* (Clarendon, Oxford, 1974).
[13] A. G. Redfield, Adv. Magn. Reson. **1**, 1 (1965).
[14] J. M. Jean, R. A. Friesner, and G. R. Fleming, J. Chem. Phys. **96**, 5827 (1992).
[15] J. C. Tully, *Modern Methods for Multidimensional Dynamics Computation in Chemistry*, edited by D. L. Thompson (World Scientific, Singapore, 1998), Chap. 2.
[16] M. F. Herman, Annu. Rev. Phys. Chem. **45**, 83 (1994).
[17] A. D. McLachlan, Mol. Phys. **8**, 39 (1964).
[18] W. H. Miller and C. W. McCurdy, J. Chem. Phys. **69**, 5163 (1978).
[19] H. D. Meyer and W. H. Miller, J. Chem. Phys. **72**, 2272 (1980).
[20] D. A. Micha, J. Chem. Phys. **78**, 7138 (1983).
[21] Z. Kirson, R. B. Gerber, A. Nitzan, and M. A. Ratner, Surf. Sci. **137**, 527 (1984).
[22] S. I. Sawada, A. Nitzan, and H. Metiu, Phys. Rev. B **32**, 851 (1985).
[23] S. Mukamel, Y. J. Yan, and J. Grad, *Stochasticity and Intramolecular Redistribution of Energy*, edited by R. Lefebvre and S. Mukamel (Reidel, Dordrecht, Holland, 1986), p. 109.
[24] G. Wahnstrom, B. Carmeli, and H. Metiu, J. Chem. Phys. **88**, 2478 (1988).
[25] M. Amarouche, F. X. Gadea, and J. Durup, Chem. Phys. **130**, 145 (1989).
[26] A. T. Amos, K. W. Sulston, and S. G. Davidson, Adv. Chem. Phys. **76**, 335 (1989).
[27] H. J. C. Berendsen and J. Mavri, J. Phys. Chem. **97**, 13464 (1993).
[28] P. Bala, B. Lesyng, and J. A. McCammon, Chem. Phys. Lett. **219**, 259 (1994).
[29] G. D. Billing, Int. Rev. Phys. Chem. **13**, 309 (1994).
[30] G. Stock, J. Chem. Phys. **103**, 2888 (1995).
[31] M. Head-Gordon and J. C. Tully, J. Chem. Phys. **103**, 10137 (1995).
[32] D. Antoniu and S. D. Schwartz, J. Chem. Phys. **104**, 3526 (1996).
[33] M. Hintenender, F. Rebentrost, R. Kosloff, and R. B. Gerber, J. Chem. Phys. **105**, 11347 (1996).
[34] J. C. Tully and R. K. Preston, J. Chem. Phys. **55**, 562 (1971).
[35] J. C. Tully, J. Chem. Phys. **93**, 1061 (1990).
[36] J. C. Tully, Int. J. Quantum Chem., Symp. **25**, 299 (1991).
[37] F. Webster, P. J. Rossky, and R. A. Friesner, Comput. Phys. Commun. **63**, 494 (1991).
[38] F. J. Webster, J. Schnitker, M. S. Friedrichs, R. A. Friesner, and P. J. Rossky, Phys. Rev. Lett. **66**, 3172 (1991).
[39] D. F. Coker and L. Xiao, J. Chem. Phys. **102**, 496 (1995).
[40] H. S. Mei and D. F. Coker, J. Chem. Phys. **104**, 4755 (1996).
[41] O. V. Prezhdo and P. J. Rossky, J. Chem. Phys. **107**, 825 (1997).
[42] C. C. Martens and J.-Y. Fang, J. Chem. Phys. **106**, 4918 (1997).
[43] C. Cohen-Tannoudji, B. Diu, and F. Laloë, *Quantum Mechanics* (Wiley, New York, 1997), Vol. 1, p. 500.
[44] S. Ross and J. P. Oliver, *Solid Surfaces and the Gas-Solid Interface*, Advances in Chemistry Series No. 33 (American Chemical Society, Washington, D.C., 1961), p. 303.
[45] D. Kosloff and R. Kosloff, J. Comput. Phys. **52**, 35 (1983).
[46] M. J. Romanelli, *Mathematical Methods for Digital Computers*, edited by A. Ralston and H. S. Wilf (Wiley, New York, 1960), Chap. 9.
[47] C. Cohen-Tannoudji, B. Diu, and F. Laloë, *Quantum Mechanics* (Wiley, New York, 1977), Vol. 1, p. 242.
[48] U. Müller and G. Stock, J. Chem. Phys. **107**, 6230 (1997).
[49] S. Hammes-Schiffer and J. C. Tully, J. Chem. Phys. **101**, 4657 (1994).
[50] E. P. Wigner, Phys. Rev. **40**, 747 (1932); M. Hillery, R. F. O'Connell, M. O. Scully, and E. P. Wigner, Phys. Rep. **106**, 121 (1984).
[51] J. C. Tully, Faraday Discuss. **110**, 1 (1998).